MECSOL 2022 - Proceedings of the 8th International Symposium on Solid Mechanics
M.L. Bittencourt, J. Labaki, L.C.M. Vieira Jr. and E. Mesquita (Editors), Campinas SP, Brazil, October 17th to 19th, 2022

Dynamic, Vibrational Analysis and Prototype sizing of Rotary Machine with Passive Magnetic Bearings

Santana, André Luís Rodrigues [1], Vieira, Izac Sousa [2], Morillo, Alfredo Hugo Valença Perazzo [3]

[1] Federal Institute of Maranhão, Colares Moreira Ave., 477 - Renascença, São Luís - MA- Brazil - Zip Code: 65075-441 - Phone: +55 86 99817-5044. andre_luis.santana@hotmail.com

[2] UniFacid Wyden University, Veterinário Bugyja Brito St., 1354 - Horto, Teresina - PI- Brazil - Zip Code: 64052-410 - Phone: +55 86 3216-7900. izacnewton1994@hotmail.com

[3] State University of Campinas, University City Zeferino Vaz., 241 – Barão Geraldo, Campinas – SP – Brazil – Zip Code:13083-970. ahvmorillo@fem.unicamp.br

Abstract: Rotary machines denote an important part of industrial society. Robust or not, they always tend to automate processes, transmit forces or make them less complex. The operation of the machines is fully connected to dynamic and vibrational forces due to high speeds and variations over time. This article designs and simulates a rotating system with magnetic bearings that discard mechanical friction, through magnetic levitation combined with low cost, ease of use and assembly. The use of free and cloud software for the creation and dynamic and vibrational simulations of the project, as well as to attest to the physical effects present in the operation of the equipment, attest to a didactic technique in dynamics. In the current context, the Frame of the machine and the printed one on ABS material facilitating its construction preventing design interference due to its versatility. Having, numerically, a flexible structure. The shaft in low density material - polycarbonate, translucent and flexible - so that it can be visualized on a micro scale that has no magnetic or mechanical interference between the bearing and shaft. In total, there are three bearings: two radial and one axial, composed of neodymium - N35. The rotating system and its components follow the Lagrangian differential equations and the Newton-Raphson Method. Natural frequencies, dynamic responses of the axis and structure are obtained. As well as the external forces, total deformation energy and kinetic energy of the shaft are calculated for the machine, thus being able to show the significant deformations due to the dynamic rotating loads of the shaft and its influence on the disc, frame and bearing assembly

Keywords: rotodynamic analysis, natural frequencies, magnetic bearing, rotating systems

INTRODUCTION

In the current context of the research, Cavalini (2017a) discusses the development of rotating systems in which they are currently employed in various sectors of industry. Steam turbines, hydroelectric plants and aircraft engines, machines that have a high cost and must have great reliability. Oliveira (2019) conducts a historical relationship about the importance and need for the use of techniques capable of optimizing the handling of equipment or available resources. According to Barbosa (2018), rotating systems are important in different areas as well as the interest and need for this type of machine. Such interest arose soon after the Industrial Revolution due to the steam engines. The first investigations on the systems had as their main objective fundamental concepts of rotational dynamics to try to minimize or overcome technical problems. According to Cavalini (2017b), the mathematical manipulations, as well as their representation, should follow via a reliable design tool such as the finite element method, MEF or FEA. This method is widely used as a technique for modeling the elements of a given dynamic rotor design. Nelson and MacVaugh - 1976 originally implemented the effects of gyroscope, rotational inertia, and axial force through the FEA model.

M. Lalanne and G. Ferraris (1998a) state that it is increasingly necessary to predict the behavior of rotors subjected to bending and torsion. First, the expressions of the kinetic and strain energies of the elements through the rotor elements and the virtual work of external forces are calculated. However, a numerical method must be introduced, and Lagrange equations applied. According to Silva (2019), the representation of a real phenomenon goes through the process of understanding and teething most coherently and efficiently possible so that the choice of information happens. The translation of this information to a problem, in an appropriate mathematical language, contributes to the understanding, equation, simulation, and the resolution of the problem.

As a result of this research, one of the relevant objectives of the bench would be the teaching of dynamics through the finding of physical effects such as gyroscope, Forwards & Backwards Whirl through computational modeling, numerical and dynamic equation. It is intended to theoretically size and understand the context of rotating machines, and dynamically,

the relationships of a rotating system composed of a passive magnetic bearing. The forms inherent in the model and its resistance and actual behavior will be validated from nodal simulations. In this way, we seek to highlight simulation models sufficiently effective to deduce the behavior of the rotating system

MATERIAL AND METHODS

Data analysis will be performed using CAD programs - Computer Aided Design and CAE - Computer dided Engineering along with sensors on the rotor, bearings and shaft available by assisted simulation platforms in which, in addition to the modeling results, they can return values of virtual sensors, approximate weight of the prototype, optimization, dynamics, excitation and magnetic force. Onshape Inc will be used in the creation and assembly process later, while SimScale will be responsible for creating the mesh and applying the finite element method. Onshape has its base entirely in the cloud and according to its platform the company has developed the only product design base that integrates CAD, PDM - Product data management, 3D and analytical services (Onshape Inc. 2020). The simulations continued via SimScale and the student versions were adopted in the programs used. The literature and research on machine dynamics served as a comparison between the behavior results obtained. The choice of numerical methods and modeling of rotating machines applying the Lagrange equations and numerical solution by the Newton-Raphson method, or Rayleigh-Ritz had as a criterion of choice the approximation with real rotating systems.

The main theoretical bases are divided according to:

- application of the finite element method;
- modeling of the rotor;
- consideration regarding the DCL of the rotor and frame;
- modeling of the magnetic bearings and dimensioning.

The rotating machine will have 1:1 full scale dimensions because it is a prototype with the intention of being compact, simple and easy to use in order to prove physical effects present in the rotating system. The shaft will have its translucent material for better verification of possible mechanical or magnetic interference. Polycarbonate due to its low mass density and transparency was introduced to the design in the axis-disc (turbine) set. The Frame frame will be made via the rapid prototyping technique. Popularly known as 3D printing and used for printing complex parts, as per Wang (2017). The general dimensions of the frame will be 600mm x 200mm x 250mm (length x width x height), according to Fig. 1. However, the internal structures that support the permanent magnets of the bearing may vary with the height or configuration used in the magnets.

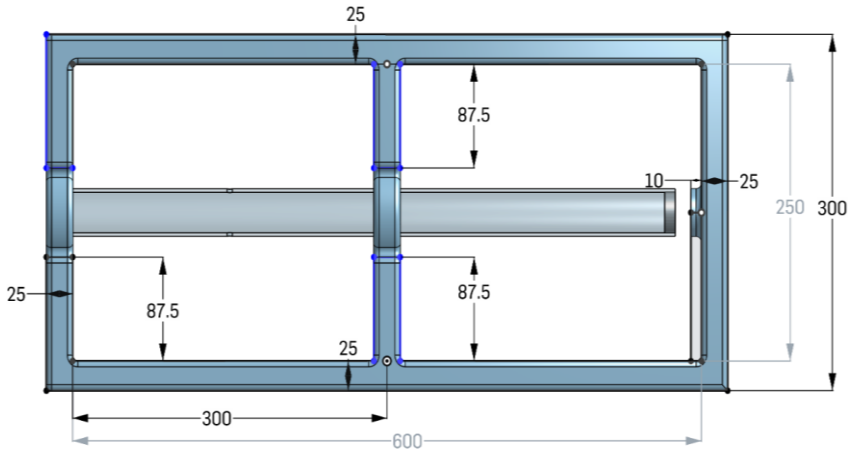

Figure 1 – Side view of the machine structure with the positioning of radial and axial bearings.

The part will be divided into three in the printing process and fitted together using connectors. The material used in the frame will be ABS - Acrylonitrile-Butadiene-Styrene, the thermoplastic most used in 3D printing, and the FDM - Fused Deposition Molding technique, which is, joining material by layers until forming the part (Aumnate, 2018). The strongest configurations currently in a magnetic magnet were chosen, the neodymium magnet with components such as neodymium, iron, and boron Nd2Fe14B. The N35 provides a considerable repulsive or attractive force that is responsible for the levitation phenomenon. Due to the low speeds achieved by the system, speed will be introduced via compressed air in the propeller turbine connected to the shaft.

Steps and Procedures

The foundation of the work is given through bibliographic research about dynamic rotor systems and rotating machines, this foundation is preponderant for the definition of methods to be adopted as well as the comparison of results with existing research. The literature review defines an important starting point in the present work, therefore, inclusion and exclusion criteria of articles, dissertations, or thesis were created, criteria that limit the time of the study, at most, to five

years for research that is not considered as the theoretical basis of the project regarding the understanding of forces, dynamics, sizing, modeling, and 3D frame. With the type of magnetic bearing used in the research and its form of application, keywords were determined for the search in digital repositories following the goals in Tab. 1.

Table 1 – Division of studies by groups and specific goals.

Research Group by Component					
Rotating system		Bearing		Shaft and Disc (Helix Turbine)	
1 – Goal	Dimensioning	1 - Goal	Bearing and Magnet Configuration	1 -Goal	Dimensioning
2 – Goal	Modeling	2 - Goal	Obtaining the magnetic forces	2 - Goal	Modeling and material
3 – Goal	Mesh design	3 - Goal	Generating magnetic force data	3 - Goal	Rotation speed
Goal	Dynamic simulation	Goal	Magnetic levitation	Goal	Rotor - low density

Mathematical Equation and Modeling

Cavalini (2013) points out that modeling a rotating system encompasses several techniques and models due to its separate components and their individual evaluation to have interpretations that are closer to the real thing because of its nature within the system. The simulations of the rotating system and its frame represent a considerable portion of this project and goal. The adopted model defines a flexible shaft with rigid bearings, one of the simplest methods to proceed with the simulations. The degrees of freedom were characterized and defined according to the tools and support material used. The equation (1), represents the differential equation of movement and dynamic behavior of the rotating system. The simplifications of the system and numerical relationship for the flexible axis are built with the general equation of movement following Lalanne and Ferraris (1998b).

$$M\ddot{v} + \left[D + \Omega D_g\right]\dot{v} + Kv = W + F_u \tag{1}$$

The equation of motion of the system takes into account the $\boldsymbol{M}$ mass matrix of the system, $\boldsymbol{D}$ the damping of the machine components, proportionally added to the damping caused by the bearing. $\boldsymbol{D_g}$ matrix responsible for demonstrating the gyroscopic effect of the system, $\boldsymbol{K}$ the stiffness matrix (all the matrices that make up the equation are connected to the rotating parts of the machine; shaft, disk, and couplings), the displacement vector or lateral vibrations of the shaft is represented by $\boldsymbol{v}$ and $\boldsymbol{\Omega}$ represents the rotational speed of the machine and its components. $\boldsymbol{W}$ represents the weight force, $\boldsymbol{F_u}$ will be the unbalance forces of the system.

Until the Eq. (1) is reached, it is necessary to determine the representative terms of each matrix or phenomenon. It is also necessary to make an analysis of each component in order to arrive at the deduction of which energy represents the element. The Lagrange Eq. (2) provide the kinetic terms for the axis, disk imbalance and mass. The axis is represented by the kinetic energies $\boldsymbol{T}$ and deformation energies $\boldsymbol{U}$ considering the influence of the unbalanced mass and the deformation energy that characterizes the axis. Virtual work is used to calculate the bearings and seals of the system. Therefore, the forces corresponding to the axis can be calculated from the general rotor equation. Where $\boldsymbol{i} = 1 < \boldsymbol{i} < N$ represents the degrees of freedom between 1 and N-Values, considering q as generalized independent coordinates of $\boldsymbol{Fq_i}$.

$$\frac{d}{dt}\left(\frac{\partial T}{\partial \dot{q}_i}\right) - \frac{\partial T}{\partial q_i} + \frac{\partial U}{\partial q_i} = Fq_i \tag{2}$$

- **T** – Kinetic energy
- $\boldsymbol{U}$ – Strain energy
- $\boldsymbol{Fq_i}$ – Generalized forces
- $\dot{\boldsymbol{q}}$ - Derived as a function of time

Lalanne and Ferraris (1998c) demonstrate the general expressions for the calculation of kinetic energy $\boldsymbol{T_S}$ and energy of $\boldsymbol{T_D}$ deformation of the shaft and disc assembly, following Eq. (3) and Eq. (4). The equation of the kinetic energy of the axis comes from a extension of Eq. 4 in a length $\boldsymbol{L}$. Where $\boldsymbol{\rho}$ and $\boldsymbol{S}$ represent the mass per unit volume is the area of the section transverse of the axis. The moment f inertia **I** and the cross-section of the axis around the neutral axis are also considered constant. Interpreting the equation from left to right, the first equation expresses the kinetic energy of an axis in bending, the second integral represents the rotational inertia, the term $\rho IL\Omega^2$ is constant, while the last integral represents the gyroscope effect.

$$T_s = \frac{\rho S}{2}\int_0^L (\dot{u}^2 + \dot{w}^2)dy + \frac{\rho I}{2}\int_0^L \left(\dot{\psi}^2 + \dot{\theta}^2\right)dy + \rho IL\Omega^2 + 2\rho I\Omega\int_0^L \dot{\psi}\theta dy \tag{3}$$

The disk is characterized by an inertial frame $R(x, y, z)$, the coordinates x, y, z are related to the inertial frame through the set of three angles $\boldsymbol{\theta}$,$\boldsymbol{\phi}$ e $\boldsymbol{\psi}$**.** Considering the symmetrical disks $\boldsymbol{I_{Dx} = I_{Dz}}$**,** the angles $\boldsymbol{\theta}$ e $\boldsymbol{\psi}$ are small is the constant

angular velocity $\dot{\phi} = \Omega$. The term $\frac{1}{2} I_{Dy} \Omega^2$ is constant, so it has no influence on the equation, but $\boldsymbol{\Omega}$ represents the energy of the rotating disk. The gyroscope effect is represented by $\frac{1}{2} I_{Dy} \Omega \dot{\psi} \theta$ and the mass of the $\boldsymbol{M_D}$ disk

$$T_D = \frac{1}{2} M_D (\dot{u}^2 + \dot{w}^2) + \frac{1}{2} I_{Dx} (\dot{\theta}^2 + \psi^2) + \frac{1}{2} I_{Dy} (\Omega^2 + 2\Omega \dot{\psi} \theta) \tag{4}$$

Shaft and disc modeling

According to Lalanne and Ferraris (1998d), the shaft is considered as a circular cross-section beam of length $\boldsymbol{L}$ is a symmetrical disc $\boldsymbol{l_1}$, with mass imbalance located on the same axis as the bearing, according to Fig. 2, having two nodes that refer to the degrees of release of the system.

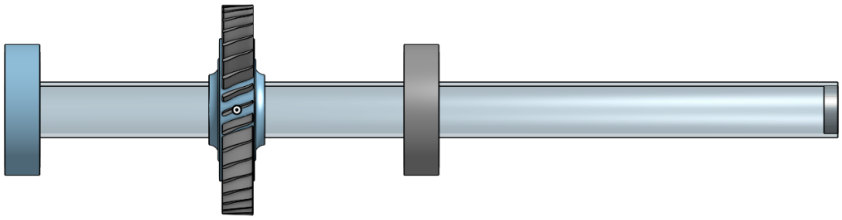

Figure 2 –Side view of the shaft and disk (Propeller Turbine).

The inertial frame is along the $\boldsymbol{Y}$ axis and the rotational speed $\boldsymbol{\Omega}$ is constant. Angular displacements $\boldsymbol{\theta}$ and $\boldsymbol{\Psi}$ can be expressed by following the Eq. (5).

$$\theta = \frac{\partial w}{\partial y}, \psi = -\frac{\partial u}{\partial y} \tag{5}$$

Due to the angular displacements being too small, the values are approximated by the following equation (6) where $\boldsymbol{q_1}$ and $\boldsymbol{q_2}$ are generalized coordinates.

$$\theta = \frac{\partial w}{\partial v} = \frac{df(y)}{dy} q_1 = g(y) q_2, \psi = -\frac{\partial u}{\partial y} = -\frac{df(y)}{dy} q_1 = -g(y) q_1 \tag{6}$$

Thus, the equations of the expression of the displacements in the **X** and **Z**, directions are respectively $\boldsymbol{u}$ and $\boldsymbol{w}$

$$u(y,t) = f(y) q_1(t) = f(y) q_1, w(y,t) = f(y) q_2(t) = g(y) q_2 \tag{7}$$

After the approximations, a representation in a second-order derivative of Eq. (6) of the expressions $\boldsymbol{u}$ and $\boldsymbol{w}$, it is necessary to formulate the expression of the deformation energy ($\boldsymbol{h(y) q_1}$ and $\boldsymbol{h(y) q_2}$) according to Eq. (8),

$$\frac{\partial w^2}{\partial y^2} = \frac{d^2 f(y)}{dy^2} q_2 = h(y) q_2, \frac{\partial^2 u}{\partial y^2} = \frac{d^2 f(y)}{dy^2} q_1 = h(y) q_1 \tag{8}$$

The axis and disk set is usually represented by the expressions of kinetic energy, so $\boldsymbol{Ts}$ for the axis and $\boldsymbol{T_D}$ for the disc. Equation (9) demonstrates how to obtain the kinetic energy present in the axis. The expression for kinetic energy originates in Eq. (6), Eq. (7) and its general formulation Eq. (3)

$$Ts = \frac{\rho S}{2} \int_0^L f^2(y) dy ({q_1}^{\circ 2} + {q_2}^{\circ 2}) + \frac{\rho I}{2} \int_0^L g^2(y) dy ({q_1}^{\circ 2} + {q_2}^{\circ 2}) - 2\rho I \Omega \int_0^L g^2(y) dy q_1 \circ q_2 \tag{9}$$

Rewriting the expression for kinetic energy Eq. (9), we have the formula for the problem Eq. (10)

$$T_S = \frac{\rho S}{2} \int_0^L (\dot{u}^2 + \dot{w}^2) dy + \frac{\rho I}{2} \int_0^L (\dot{\psi}^2 + \dot{\theta}^2) dy + 2\rho I \Omega^2 + 2\rho I \Omega \int_0^L \dot{\psi} dy \tag{10}$$

The propeller turbine is considered ideally and rigid so that there is less variation of possible errors of the equations generated by each finite element in the application of the method. The strain energy is used to express the values and phenomena that occur with the disk, exposed in Eq. (11). Just as the expressions for the kinetic energy of the axis originate in the Eq. (6) and Eq. (7), the kinetic energy for the disk originates from the same equations, but based on the general of disk Eq. (4)

$$T_D = \frac{1}{2} [M_D f^2(l_1) + I_{DX} g^2(l_1)] ({\dot{q}_1}^2 + {\dot{q}_2}^2) - I_{DY} \Omega g^2(l_1) q_1 \circ q_2 \tag{11}$$

The total kinetic energy of the shaft and disk assembly can be obtained by adding the equations expressing the kinetic energy of the disk and shaft, Eq. (12).

$$T = T_D + T_S \tag{12}$$

$$T = \frac{1}{2}\left[M_D f^2(l_1) + I_{DX} g^2(l_1) + \rho S \int_0^L f^2(l_1)dy + \rho I \int_0^L g^2(y)dy\right]\left(\dot{q}_1{}^2 + \dot{q}_2{}^2\right) - \Omega\left[I_{DX} g^2(l_1) + 2\rho L \int_0^L g^2(y)dy\right]$$
$$q_1{}^{\circ}q_2 \tag{13}$$

By simplifying the expression of total kinetic energy, we obtain the compact form Eq. (14)

$$T = \frac{1}{2}m(q_1{}^{\circ 2} + q_2{}^{\circ 2}) - \Omega a q_1{}^{\circ}q_2 \tag{14}$$

Magnetic Bearing Modeling

Lalanne (1998e) assures that this modeling is the virtual work principle for bearings. The procedure would proceed by the following Eq. (15).

$$\delta W = -k_{xx}u(l_2)\delta u(l_2) - k_{xz}w(l_2)\delta u(l_2) - k_{zz}w(l_2)\delta u(l_2) \tag{15}$$
$$-k_{zx}u(l_2)\delta w(l_2) - c_{xx}u^{\circ}(l_2)\delta u(l_2) - c_{xz}w^{\circ}(l_2)\delta u(l_2)$$
$$-c_{zz}u^{\circ}(l_2)\delta w(l_2) - c_{zx}u^{\circ}(l_2)\delta w(l_2)$$

Replacing Eq. (7) and Eq. (15), we obtain a compact expression for virtual work with generalized terms of the forces acting on the axis

$$\delta W = Fq_1\delta q_1 + Fq_2\delta q_2 \tag{16}$$

Due to the characteristic stability of levitation by permanent magnets, it is not possible to balance the rotor with three degrees of freedom, requiring the use of techniques and strategies different from the Standardized for mechanical bearings (Yamamoto and Fumagalli, 2019). The model, magnetic bearing, calculation of forces, axial force, rigidity and techniques. Used are based on works already carried out starting with Yonnet (1981a) and Qian *et al*. (2003). Due to the complex calculations of the magnetic medium, the configurations were made according to the Purpose of this study. To start calculating the forces that act along the magnets, it is necessary to define three hypotheses. Ideal for behavior and structure, thus making the calculation of magnetic flux and field Simplified magnetic, according to Yonnet (1981b).

RESULTS AND DISCUSSIONS

Shaft and disc modeling

Numerical results are values generated and necessary during the simulation process. Demonstrating the interactions of the equations of resolution, time, number of matrices, misinterpretation due to lack of force parameters, and excessively restricted degrees of freedom at the time of definition in contrast to material characteristics.

The absolute or relative residuals are used internally and numerically by the software in dynamic analyses to arrive at a convergence value in the solution methods. The relative residual follows the Eq. (17) in which it shows a problem if the external force equals zero. During a specific period of the simulation an error or process failure occurs, which shows that no external load is being applied at that instant and it is necessary to apply an absolute residual according to Fig. 3. B.

$$R_r = \frac{(Internal\ forces - External\ forces)}{External\ forces} \tag{17}$$

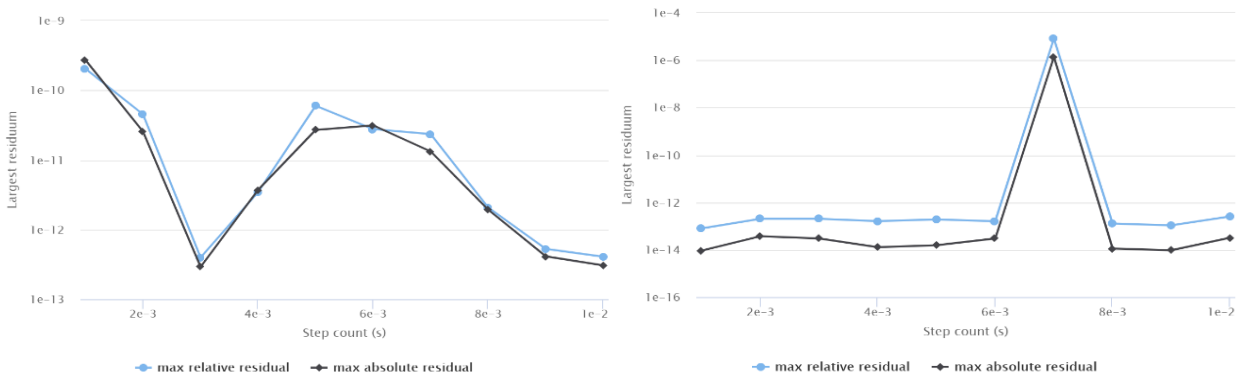

Figure 3 – (A) Graph with the maximum relative and absolute residuals from the Frame dynamic analysis, (B) Graph with the maximum relative and absolute residuals from the shaft dynamic analysis.

It can be observed that between 6.10^{-3} and 8.10^{-3} s there is a peak followed by a valley of the absolute and maximum residuals, demonstrating a space of time during the simulation that no external loads were observed, so the increase in the residuals is aimed at making the method converge again and the simulation does not fail. But one can notice a constancy in most of the applied residuals unlike the dynamic analysis of the shaft in Fig. 3. A. The variation and instability of the residues applied to the shaft between 2.10^{-3} - $4x10^{-3}$ s and 6.10^{-3} - 1.10^{-2} s show a decay of the residue applications starting from the order 1.10^{-9} with a minimum value between 1.10^{-12} - 1.10^{-13} this instability is understood to be due to shaft speeds and flexibility and lateral vibrations.

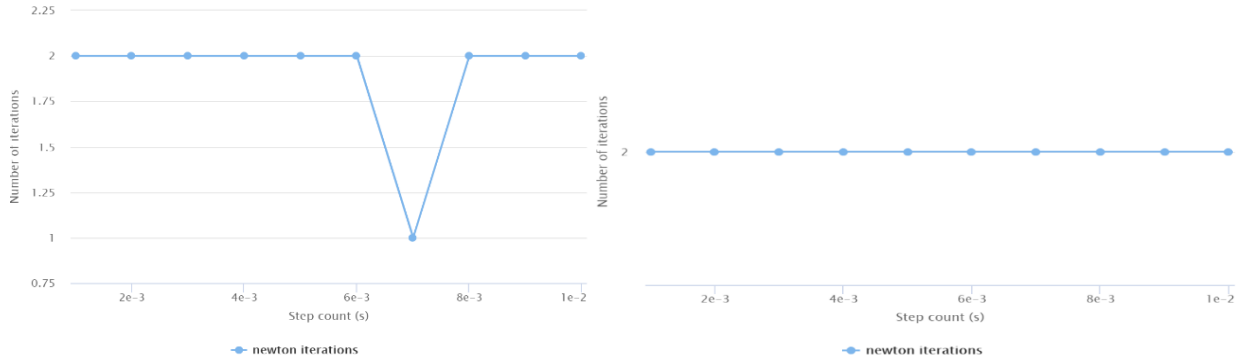

Figure 4 – (A) Graph with Newton's interactions from the Frame dynamic analysis, (B) Graph with Newton's interactions from the shaft dynamic analysis.

Newton's interactions and a method for solving equations but diffused as the Newton-Raphson method. Figure 4. A show's the number of interactions in the frame during a time interval of the equations or steps until the total resolution of the simulations, numerical to completion. Between 6.10^{-3} - 8.10^{-3} s the interactions demonstrate a non-convergence of the method. Comparing Fig. 4. A and Fig. 3. B it is noted a similarity between the graphs in which the instant 6.10-3 - 8.10-3 s coincide in the time interval and opposite ways demonstrating that as the non-convergence increases there is a greater application of the relative, absolute maximum residuals in the attempt to return to the convergence of the method.

Newton's interactions reflect a state of non-convergence of the method for periods of time without applied load. Figure 4. B demonstrates the interactions or operations for solving the differential equations every $2x10^{-3}$ keeping throughout the simulation a constant convergence with two interactions differently from Fig. 4. A the one that represents the Frame, one can notice a valley reaching one iteration per second. Lalanne and Ferraris (1998f) demonstrate the shaft through the strain energy and kinetic energy through Eq. (10), (11). Fig. 5 shows total external work as a function of kinetic energies, strain energy, connection energy, damping dissipation, and numerical dissipation.

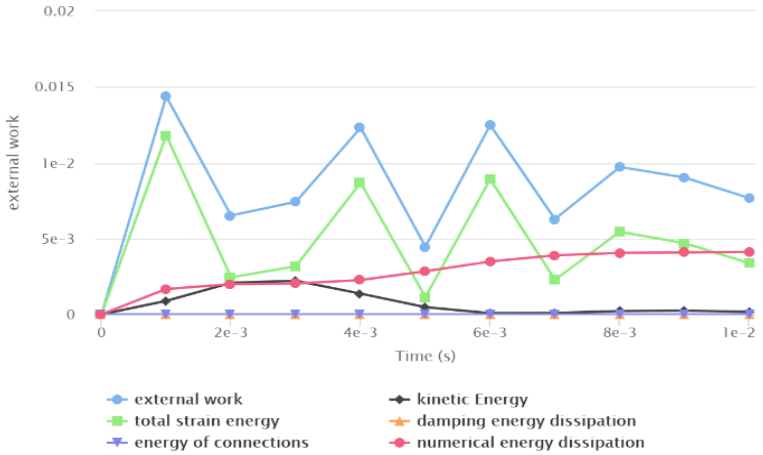

Figure 5 – Graph with the variations of values of the total external and internal work from the dynamic shaft analysis.

Printed Frame Analysis

The machine has three different materials ABS, neodymium, polycarbonate Frame material, turbine, magnetic magnets, and the shaft that is connected with the rotor and bearings, both responsible for power transmission. The Tab. 2 shows dimensional values of the machine frame.

The algorithm for mesh generation was the standard one, which is indicated for both fluid mechanics and solid applications due to the number of nodes and mesh refinement, as shown in Tab. 3. For this reason, it was decided not to choose the tet-dominant mesh with its main tetrahedral elements because it was already considered sufficiently capable of reaching a real convergence. Through the mesh dimensioning it was decided to leave it automatic so that the algorithm would create and traverse with the necessary size and granularity each point of the bench.

Table 2 – General frame data after optimization.

Frame Dimensional Data								
	Momento of inertia – $kg.m^2$					Mass	Volume	Surface
Lxx:	0.334	Lxy	$3.200.10^{-7}$	Lxz:	$-1.784.10^{-7}$			
Lyx	$3.200.10^{-7}$	Lyy	0.081	Lzy	$5.031.10^{-5}$	5.998 *kg*	0.005 m^3	1.018 m^2
Lzx	$-1.784.10^{-7}$	Lzy	$5.031.10^{-5}$	Lzz	0.285			

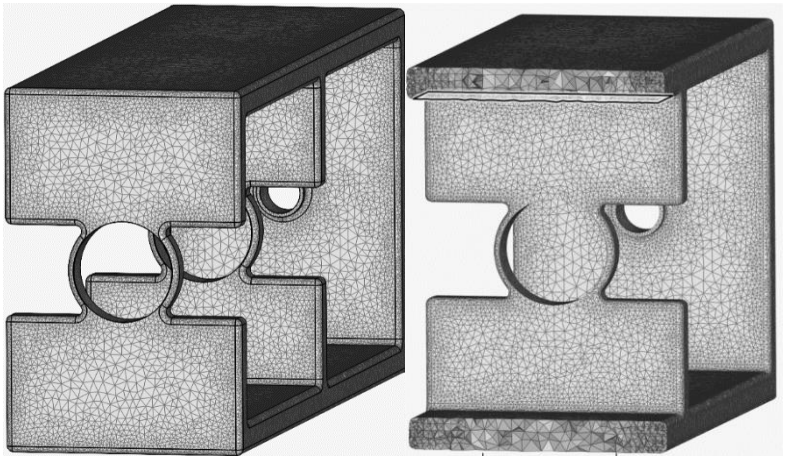

Figure 6 – Frame in perspective after mesh generation (A), Section view, and mesh refining (B).

The mesh generation time was around 10 to 15 minutes. According to the log solver, the mesh has an accuracy of the order of 2.508201303281464.10-7 m. The mesh is divided into geometric sets that are solved separately via matrices - *tetEdgeRatio*, *triMaxAngle*, *triMinAngle*, *volumeRatio*, *tetAspectRatio*, *nonOrthogonality*, *skewness*, *aspectRatio*. The overall quality of the mesh based on the 99% percentile is 0.6527.

Table 3 – Automatically generated mesh data according to the structure.

Frame Mesh Generation Data			
Number of nodes	Number of faces	Number of triangles	Number of tetrahedrons
190690	118540	118540	924130

Due to the lack of research and works that have the same structural characteristics, it was decided to wait for the second part of the research, this experimental phase, so that the data could be collected with greater precision and, thus, redo the dynamic tests. For the dynamic analysis to converge, standard values were adopted - load based on a safety factor for the dynamic test of the frame, considering that the nodal test does not require any external load to the body.

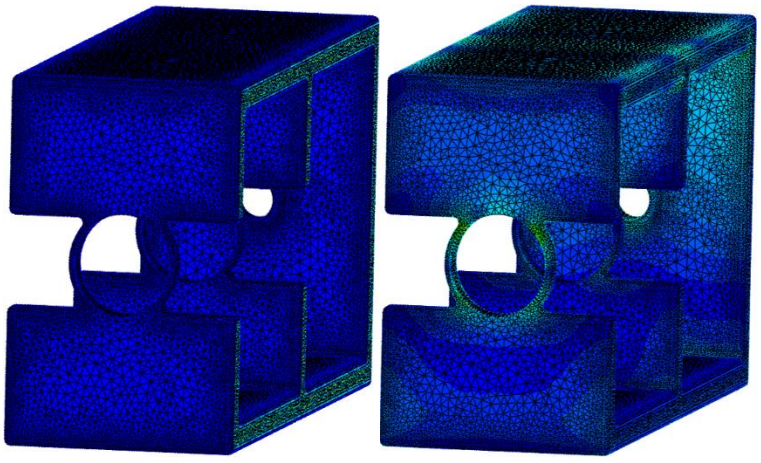

Figure 7 –Total accelerations present in the Frame - *m/s²* (A), Stress or Von Mises stress - Pa (B).

Figure 4 shows the behavior of the structure with the application of -30 Newton at the most vulnerable points of the structure purposely across the span, which goes between the first and third axial bearing. Cooler colors represent area of lower stress or displacement, and warmer colors represent points of higher stress. A greater variation can be seen in Fig. 7. B, the speeds varied from 0.00136237 m/s^2 - 424.775 m/s^2 while the stresses 23.91 - 13986 Pascal. A few points or nodes are highlighted where they tend towards red - areas of greater stress, but overall, the behavior of the structure is efficient.

Table 4 – Vibration modes of the frame and its natural frequencies.

Vibrate Modes and Natural Frame Frequencies - Hz									
1	2	3	4	5	6	7	8	9	10
148.32	148.58	148.99	149.47	150.53	152.14	162.75	164.12	177.18	201.46

The natural frequencies of a body do not necessarily require a value to reach convergence or values differently from harmonic simulations. Fig. 7 demonstrates the first and last frequency of the body, meaning the total displacements. Fig. 7. B varies from 0.002241 - 1.323 m, however, from Fig. 7. A - B 0.00257 - 1.029 m small variations are noticed showing that if reaching any of the frequencies the structure may collapse. In the first mode, there are no significant deformations, however, it is noticeable an excessive accumulation of stress on the faces of the last axial bearing.

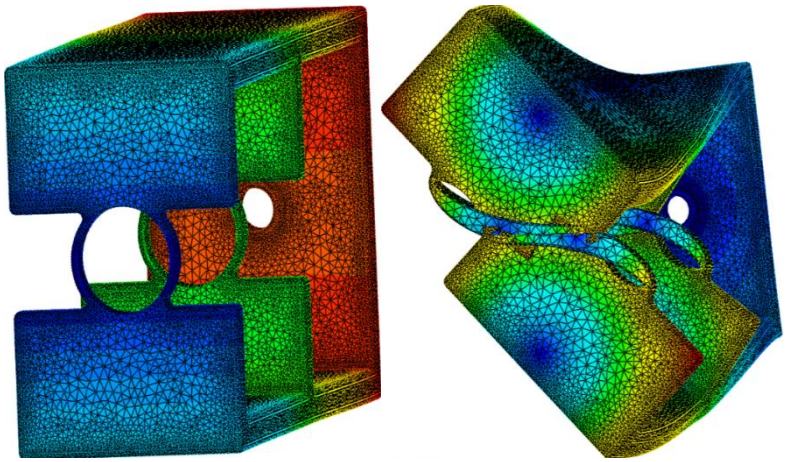

Figure 8 – Deformations of the natural frequency of the structure in the first mode of vibrating 148,328 Hz (A), tenth mode of vibrating (B) 201,466 Hz.

Axis analysis

It was decided to leave the automatic meshing as this is already considered efficient for data convergence, thus saving memory and machine time. The mesh order defines the number and shape, according to the logarithm mapping, so there is no need to choose second order elements for even more accurate results.

Table 5 – Automatically generated mesh data according to the structure.

Axis Mesh Generation Data			
Number of nodes	Number of faces	Number of triangles	Number of tetrahedra
1965	3930	3930	5656

Comparing the numerical data of mesh generation with the Frame, a large difference is observed due to the dimensions and energies that act on the elements, requiring surfaces with greater mesh refining.

Table 6 – Vibration modes of the axis and its natural frequencies.

Vibration Modes and Natural Axis Frequencies - Hz									
1	2	3	4	5	6	7	8	9	10
1136.91	1136.92	1138.19	1138.2	1139.17	1147.67	1147.72	1201.49	1202.07	1250.4

The dynamic analysis was performed, and the numerical results are available in the topic (Shaft and disc modeling). Due to the characteristics and main objective, it was decided to focus on the natural frequencies of the body in view of the fact that the axis already has a large dynamic variation for being in continuous motion.

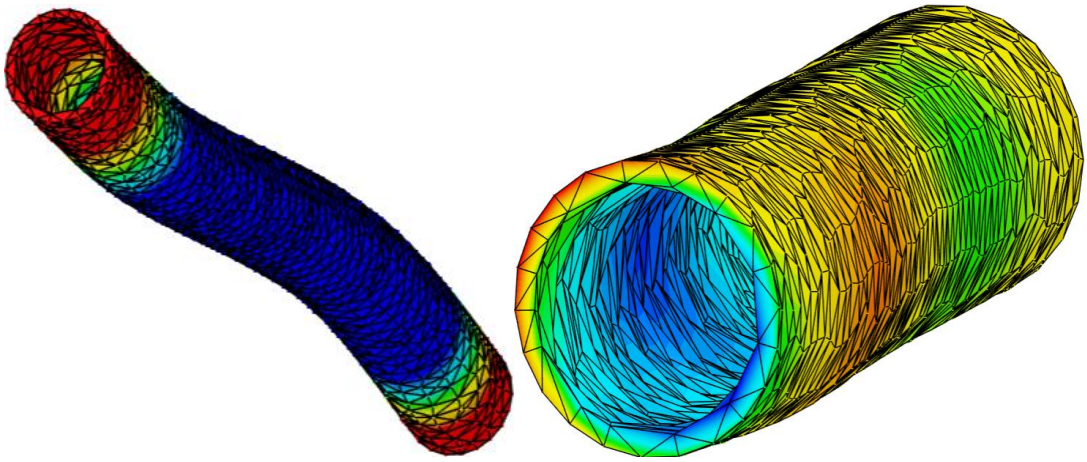

Figure 9 – Deformations of the natural frequency of the shaft in the first mode of vibrating 1136.91 Hz (A), tenth mode of vibrating 1250.4 (B) Hz.

Higher natural frequencies are noted for shaft Tab. 6 than in Frame Tab. 4. Due to the greater dynamic variations and rotations that the axis is exposed to. The total displacements Fig. 9. between a range of 0.702 - 1.023 m are equal to the displacements experienced in Fig. 9. B. The variations in ***x***, ***y*** and ***z*** are simulated by the software but it was chosen to show total values.

Analysis of Orbits and Gyroscope Effect

The axis, being hollow and flexible, shows already expected vibration modes and deformations that make the structure unfeasible. But, as the frequencies increase, an increase in its diameter and crushing of the axis is observed, decreasing its length, as shown in the Fig. 9. A and Fig. 9. B. Figure 10. A demonstrates the force vectors and their direction in which the structure tends to deform.

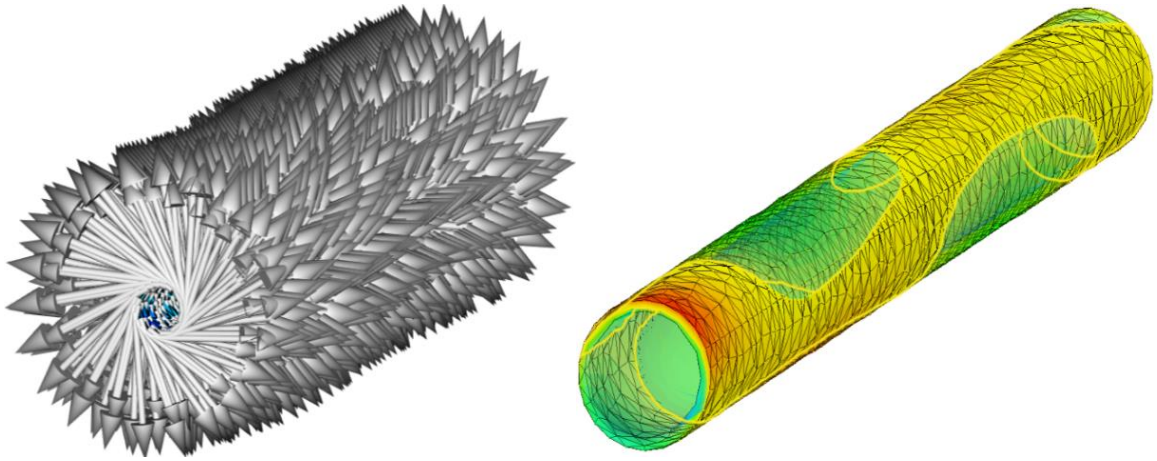

Figure 10 – Displacement vectors in the tenth mode of vibrating (A), mapping of the intermediate area algorithm (B).

The gyroscope effect is characterized by an increase in the diameter of the axis due to the increase in speed. Simon (1982) states that the gyroscope effect increases the natural frequencies when having a forward's motion. The natural frequencies are interconnected to the gyroscope effect as well as the forwards & backwards whirling orbit effects that in addition to the body frequencies, frequencies are generated for each orbit. However, it is possible to validate the gyroscope effect present on the axis and the direct precession movement.

CONCLUSION

The study of rotor dynamics and its components still represents a small portion of the many unknowns present in the approximation of simulation with the real thing. This article adds techniques, methods, and results to the area, contributing to the technological advancement of rotating machines and magnetic bearings - levitation. It was decided to divide the study into two parts due to the difficulties caused by the worldwide pandemic and complexity of the proposed study. The current part consists of the dimensioning phases and simulations generating data for comparison with the real thing, while the experimental part is understood to be a second article based on the first one that is being used as a graduation object.

The machine was developed to be easy to use, transport, assemble, low cost, and visualize the orbits and present effects of dynamics and vibrations. Thinking about this, the academic difficulties, and the high monetary value of CAD and CAE programs, the use of cloud-based software and with free licenses. Thus, they denoting a key for teachers in teaching the dynamics or in projects and simulations, making its didactics efficient.

The most robust part of the machine is the ABS printed frame. The dynamic responses were satisfactory for the stipulated load with only points or stress concentrating finite elements, not denoting a collapse of the structure due to the loads. However, in the nodal analysis natural frequencies showed significant deformations from the first vibration mode as already expected in radial bearings. The resonance action on the structure may be difficult to be achieved due to the dynamic loads being minimized in the structure by the presence of magnetic levitation and thus no mechanical contact with the frame is obtained, decreasing the action of the dynamic loads present in the speeds on the axis.

Because the axis is arranged over bearings that do not achieve stability static, this axis is represented by springs that act with different stiffness coefficients. It was found that the adoption of diamagnetic materials would make the process conceptually more effective, however, the budget would be out of standards. As there are six degrees of freedom in the bearing for which a degree of has been minimized with the axial axis, the modes of vibrating have high amplitudes and considerable displacements can also be perceived through simulations. The gyroscope effect present in the structure can be ascertained through the force and displacement vectors of the structure that tend to increase the diameter of the axis directly connected with the orbit forwards - direct precession. The experimental phase and the introduction of sensors in the structure made the study more reliable and complete, allowing it to be compared with the stipulated and simulated data closer to reality. The collapse caused by the natural frequencies on the shaft compared to the Frame can be more destructive due to the lateral vibrations suffered by the shaft that directly affect its equilibrium thus favoring disbalancing of the propeller turbine mass – Disk.

The dimensioning and choice of material was based on the criteria of materials with a low density per length, making the system portable and easy to assemble, making the levitation of the shaft more sufficient and taking into consideration that the height or width of the external magnet should be much greater than the space between the external and internal magnet - radial bearing and shaft. The configuration containing the axial shaft with radial magnetization was found to be more efficient due to the greater free action of the magnetic forces reconciled with the ring bearings.

The numerical results for both the shaft and the structure used the Newton-Raphson method to solve their differential equations, which showed good results. A complex portion of the study and simulations of rotating machines is understood within the numerical modeling and interpretation of the forces present in the shaft, bearing, and disk. The insertion of magnetic bearings and the levitation principle was a challenge, having to combine classical equations of rotor modeling with the attraction or repulsion forces of the magnets.

REFERENCES

Aumnate, C.E.A., 2018, “Fabrication of abs/graphene oxide composite filament for fused filament fabrication (fff) 3d printing”, Advances in Materials Science and Engineering, V. 2018, p. 242–246.

Barbosa, P. C.P.F., 2018, “Dynamic behavior analysis of composite material shafts in rotating machines”, Master’s thesis, Federal University of Uberlância, Minas Gerais, Brazil.

Cavalini JR, A.A., 2013. “Detection and identification of incipient cross cracks on flexible horizontal shafts of rotating machines”, 235f, Doctoral thesis. Federal University of Uberlância, Minas Gerais, Brazil.

Cavalini, JR. A. Ap., *et al*., 2017, “analysis of the dynamic behavior of a rotating composite hollow shaft”, Latin american journal of solids and structures, v. 14, Federal University of Uberlândia, Minas Gerais, Brazil, p. 1-16.

Fumagalli, M.A., Yamamoto, R.I., 2019, “Magnetic Bearings: Concept and Application”, FTT-Journal of Engineering and Business, v. 1, São Bernardo do Campo, Brazil, n. 4

Lalanne, M. e Ferraris, G., 1998, “Rotordynamics prediction in engineering”. John Wiley & Sons, INC.

Oliveira, M.V.F.D., 2019, “Flexible Rotor Control Supported by Magnetic Bearings”, Doctoral thesis, Federal University of Uberlândia, Minas Gerais, Brazil.

ONSHAPE INC., 2020, “Product Design Platform That Combines CAD, 3D, PDM”, Cambridge, Massachusetts, EUA.

Silva, S.J., 2019, “Rotating machine dynamics: a learning tool in high school”, Master’s thesis, Federal University of Goiás, Brazil, 66 p.

Simon, T., 1982, “Dynamic stressing of Hydro Electric Units by Stochastic Hydraulic Forces on the Turbine Runner”, International Water Power and dam Construction, v.29, n.1, p.39-44.

SIMSCALE., 2020, “Full cloud CAE software that helps perform CAD model simulations”. Munich, Bayern.

Wang, X. E.A., 2017, “3d printing of polymer matrix composites: A review and prospective”. Composites Part B, v. 110, p. 442–458.

RESPONSIBILITY NOTICE

The author(s) is (are) the only party(ies) responsible for the printed material included in this paper.